Flux and Nuclear Heating Rate Calculations for CALORRE Irradiation in MITR

S. Hauptman[1,*], A. Volte[2], G. Kohse[1], M. Carette[2], A. Lyoussi[3], C. Reynard-Carette[2]

[1]Massachusetts Institute of Technology, Nuclear Reactor Laboratory, Cambridge, Massachusetts, USA
[2]Aix Marseille Univ, Université de Toulon, CNRS, IM2NP, Marseille, France
[3]CEA/DES/IRESNE/DER, Section of Experimental Physics, Safety Tests and Instrumentation, Cadarache, F-13108, Saint Paul-lez-Durance, France

(*) hauptman@mit.edu

***Abstract*— This work summarizes neutronic calculations performed for the CALORRE differential calorimeter specifically designed by Aix Marseille University to inform the irradiation campaign planning for testing in MITR within the framework of the CALOR-I research program. MCNP software was used to predict the neutron and gamma flux spectrum, and total nuclear heating rate to the components of the calorimeter in a variety of positions. Results were compared to evaluate spatial bias, core loading effects, optimization for axial position, and provide input data for thermal multi-physics modelling.**

***Keywords* — Calorimeter, Nuclear Heating Rate, Neutronics.**

I. Introduction

The CALOR-I research program, (compact-CALORimeter Irradiations inside the MIT Research Reactor) began in 2020 within the framework of the joint LIMMEX laboratory between Aix Marseille University (AMU), the CEA and the CNRS. This program is funded by A*Midex Foundation. It is led AMU and involves two partners: the Nuclear Reactor Laboratory at MIT and the CEA. The first two aims of this program focused on design of a new compact prototype of the CALORRE calorimeter [1] and performance of realistic condition testing in laboratory thanks to calibration protocol, both of which have been successfully completed. The final goal is to test a dedicated in-core water loop multi-sensor device in the MIT Research Reactor (MITR) to verify measurement performance and validate the predicted nuclear heating rate using the new reduced-size prototype of CALORRE by imposing several conditions (reactor power levels, convection intensity) and by applying different measurement methods.

In order to support the completion of this project, accurate predictions of the in-core environment and the effects on components are needed to inform irradiation campaign planning and instrumentation design. These predictions investigate the energy spectrum for both the neutron flux and gamma flux in a representative volume, the total heating rate expected in the materials, and the potential for spatial bias and core loading effects to influence the measurement.

II. Description

A. MITR Water Loop Facility

The Massachusetts Institute of Technology (MIT) Research Reactor (MITR), is a light-water cooled and moderated tank-type reactor, licensed for operation up to 6 MW_{th}. The MITR has several experimental facilities, including three in-core positions for irradiation over a 10-week operating cycle. The position of interest for the CALOR-I project is the B3 position, in the middle ring of the core which is designated for high-temperature water loop (HTWL) facilities. A mockup of the core tank with the HTWL seated in the upper and lower grid plate is shown in Figure 1.

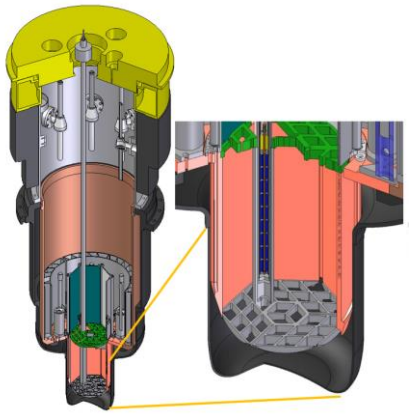

Fig. 1. Diagram of installed HTWL facility in B3 position. Fuel elements are omitted for clarity.

The HTWL allows for accurate control of in-core experiment temperature and flow conditions while exposing the installed sample components to high neutron and gamma flux. A unique feature that makes MITR an ideal choice for testing is the similar flux spectrum and power density to a commercial pressurized water reactor (PWR) core. The independent water loop provides the control functions to tailor the coolant chemistry, temperature, flow, and pressure to desired experimental conditions without adversely affecting MITR operation [2].

B. Calorimeter

The CALORRE capsule is composed of two calorimetric cells (a sample cell and a reference cell). Each cell has a central alumina and nichrome heating element, a structural holder, and

8 equally spaced fins connecting the cell to the outer wall of the calorimeter capsule. The sample cell has the stainless-steel material (SS316L) of interest between its heater and fin ring, and the reference cell leaves a gap around the heating element to be filled by di-nitrogen. The cells are superimposed and are 29.55 mm apart. The various thermocouples (2 per cell) and connection wiring (4-wire heater) will be routed through the inside of the capsule and out the top to connect back to the measurement system outside the core. The calorimeter capsule will be placed thanks to a specific device in the water loop autoclave which is monitored by its own MITR controllers and indications [3].

III. Model Parameters and Methodology

A. Model Assumptions

Nominal STP densities were used for the modeling of the capsule components. Figure 2 shows the comparison between the mechanical model and the visualization of the geometry in the MCNP input deck. The smaller instrumentation masses of the wires and thermocouples were neglected from the neutronic input deck as they are unlikely to impact the tally results of the larger components. The fixtures and structural supports holding the capsule itself in place in the HTWL were also neglected due to their distance from the region of interest. The top plug of the capsule and the nose cone have non-negligible mass by comparison and were included, the shape of the capsule and more specifically the displacement of the water volume within the HTWL was preserved.

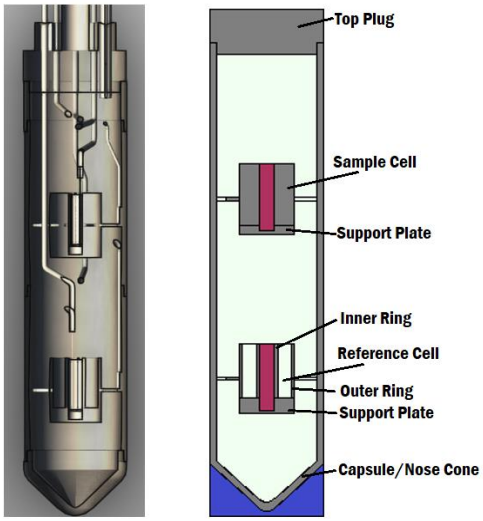

Fig. 2. CAD drawing (left-hand section) created by A. Volte, converted into MCNP input geometry (right-hand section) with labels corresponding to component designations for nuclear heating rate results.

B. Neutronic Problem Settings

The problems were all run in MCNP5 v1.60 using ENDF-VII nuclear data libraries [4, 5]. Comparison checks were done with MCNP6.2 using the same data resources to confirm agreement and compare different tally methodologies. MCNP6 was also used to verify the energy component due to electron deposition can be reasonably assumed using the default local deposition settings. For a coupled neutron-photon problem, MCNP5 was selected due to the reduced runtime. F6 neutron and gamma energy deposition tallies were used in order to separate the heating contributions.

Each problem was run with 800 active cycles and 800,000 neutron histories per cycle to obtain tally statistics with low uncertainties, particularly for the fin geometries. The CALORRE capsule components are geometrically very small and the fins relatively thin, which required more simulation time to satisfactorily converge. Additional random seeds were used and the resulting tallies merged for further variance reduction.

C. Normalization

All tally results were normalized to a reactor power of 6 MW. Measurements during the irradiation campaign may be performed at various power levels but the correction to lower power is linearly proportional and does not require separate simulation results. MCNP does not have the capability to track energy deposition from the delayed gamma component. However, the total gamma heating rate for MITR in-core irradiations can be calculated using established coefficients following (1) [6].

$$\gamma_{total} = \gamma_{prompt} + \gamma_{delayed} = 1.53 * \gamma_{prompt} \quad (1)$$

D. Problem Setup

The axial flux profile across the MITR core is not sharply peaked but has a changing gradient. To account for differences as a function of height, pairs of problems were run centering first the sample cell and then the reference cell at a fixed axial point. Five locations were chosen 5 cm apart ranging from 15 cm below the core centerline to 5 cm above the core centerline. These comparison predictions allow for a best estimate of the correction factor that may need to be applied during the actual measurement to obtain the net difference in measurements between the two cells of the calorimeter.

It was also investigated to see if local fuel loading had a notable effect on the calculated heating rates. Unlike most other reactors, MITR does not have a fixed fuel loading or shuffling pattern and both the burnup and orientation in the elements that border the B3 experimental position can vary between operating cycles. Four core loading patterns that were representative of typical loadings and included the different potential configurations of the border elements were used. The power output for each nodalized section of the closest fuel plates was calculated and compared to the resulting total nuclear heating rates.

The other area of investigation concerned the orientation of the fins. The B3 position is not directly in the center of the core and although it receives a relatively uniform radial flux, both neutron and gamma, if there is a directional component influencing the total nuclear heating rate it could necessitate adding rotation to the facility design and irradiation campaign. The nuclear heating rates were calculated in each individual fin for two capsule positions: one in the peak flux position with the sample cell centered at 5 cm below the core centerline, and one in a low flux position with the sample cell centered 15 cm below the core centerline. For these two axial positions, a problem run

was tallied with five different starting random seeds and four different core loading files.

IV. RESULTS

A. *Flux Profiles*

The neutron and gamma flux profiles seen by each of the capsule components, matches closely with the known flux profiles for MITR in-core positions. The total neutron flux, shown in Figure 3, has a peak around 2.4 $x10^{14}$ n. $cm^{-2}.s^{-1}$ and drops to 1.2 $x10^{14}$ n. $cm^{-2}.s^{-1}$at the higher core planes. The higher the total flux, the more tightly the values for each component are clustered. This again follows the known core profile trends where the flux gradient is lowest across the peak region, and increases towards the bottom and top of the active core.

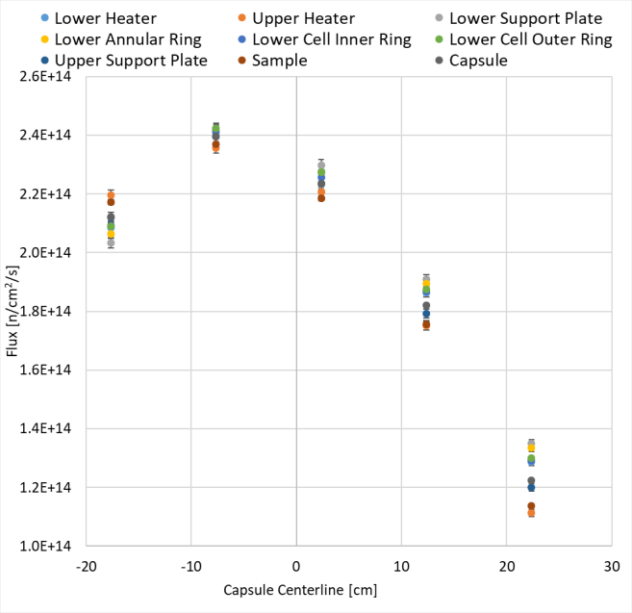

Fig. 3. Neutron flux in capsule components over several axial positions with 1σ error bars.

In Figure 4, the gamma flux also peaks at the same core height and displays a similar clustering and gradient behavior, but is overall less peaked and more uniform throughout the core.

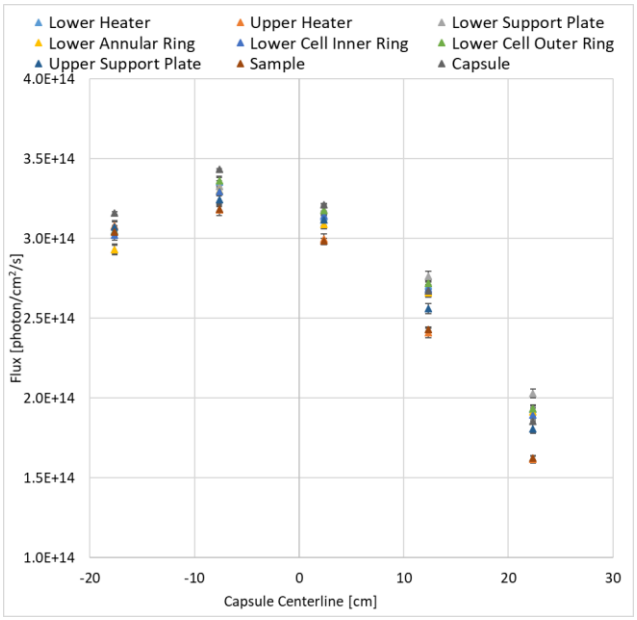

Fig. 4. Gamma flux in capsule components over several axial positions with 1σ error bars.

The gamma spectrum was also tallied at four quadrant locations on the exterior of the capsule to investigate any local shielding effects that might occur and how that could influence the placement of a second independent measurement to be performed by a commercial gamma thermometer. The spectrums were nearly identical which supported no physical limitation on radial positioning as the gamma flux is negligibly perturbed by the calorimeter.

B. *Nuclear Heating Rates*

The total nuclear heating rates across all non-fin SS316L components and positions for the statistical combination of tallies, ranged from 1.59 ± 0.02 $W.g^{-1}$ to 2.01 ± 0.02 $W.g^{-1}$. All non-fin heating rates as a function of capsule position are shown in Figure 5. The relative order of which component saw the highest heating also was fairly consistent above the peak flux point and below it. The expected inversion across the plane of peak flux, about 5 cm below the core centerline, was observed as the reference and sample cells switch which one is closer to the higher flux point (i.e. in the top half of the core it is anticipated that the reference cell will see more heating, whereas in the bottom half of the core the sample cell is expected to see more heating).

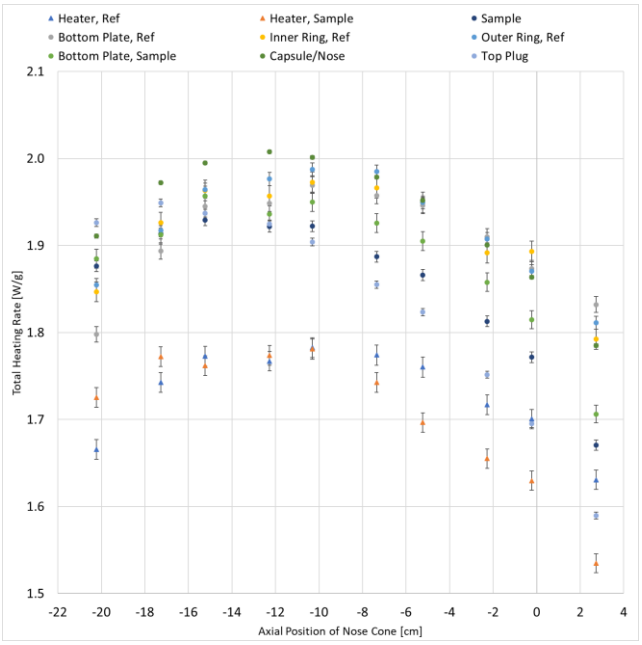

Fig. 5. Total nuclear heating rates in each component over several axial positions. Nuclear heating rates have been calculated from the statistical combination of three random seed runs and normalized to 6 MW.

C. *Bias Checks*

Figure 6 shows the fin designation with respect to core position as well as the positions bordering B3. Despite the different node power outputs and orientations between the neighboring element positions in core configurations 238, 239, 240, and 242. An example of the variation in power profile is demonstrated by the 10th axial nodes for core configurations #240 and #242 in Figure 7. No impact was observed on the calculated nuclear heating rates tallied in the fins. Particularly of note is the core loading of #240 with the C5 element in a different posture and an inverted power distribution throughout the plates did not impact the local heating rate.

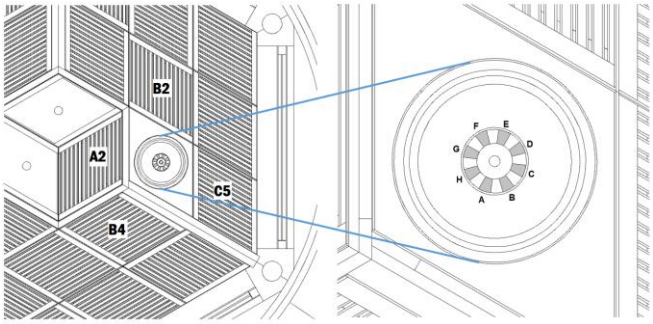

Fig. 6. Cross section of CALORRE capsule in B3 core position (left-hand section) with zoomed in image (right-hand section) showing sample cell fins and label designation for orientation. Positions of neighboring elements are also labelled.

240					242			
A2	B2	B4	C5		A2	B2	B4	C5
1489	1383	1517	1789		1568	1432	1466	1077
1411	1346	1472	1450		1508	1337	1407	1055
1363	1353	1468	1249		1468	1335	1389	1016
1380	1319	1422	1133		1463	1328	1360	988
1383	1299	1405	1086		1425	1310	1346	1020
1390	1307	1412	1043		1440	1322	1345	1007
1366	1311	1423	1012		1421	1320	1313	992
1361	1322	1389	1034		1432	1355	1341	1008
1339	1315	1374	1025		1451	1323	1296	1005
1352	1343	1367	1052		1438	1347	1297	1044
1344	1358	1318	1023		1452	1376	1294	1016
1402	1390	1346	1081		1470	1408	1322	1019
1390	1380	1393	1098		1463	1422	1317	1057
1393	1427	1445	1152		1466	1447	1352	1039
1454	1522	1521	1232		1557	1514	1427	1033

Fig. 7. Power profiles of node 10 of each neighboring fuel element to B3, for two of the four analyzed core loadings (#240 and #242). The 10th node borders the sample cell with the capsule in the high flux position, encompassing the -7.104 cm to -3.552 cm axial section. Power output values for each of the 15 fuel plates are listed in watts and normalized to nominal operating power of 5.7 MW.

The nuclear heating rate results of the two flux positions chosen for fin bias checks are given in Figures 8 and 9, for the high flux and low flux positions respectively. In each, the highest predicted nuclear heating rates are shown in red and the lowest in blue.

	Reference Cell				Sample Cell			
Core	238	239	240	242	238	239	240	242
A	1.95	1.96	1.96	1.96	1.94	1.92	1.97	1.98
B	1.93	1.92	1.96	1.99	1.92	**1.89**	1.95	1.94
C	1.94	1.96	1.97	1.95	1.92	1.91	1.96	1.96
D	**1.91**	1.95	1.97	1.95	1.91	1.92	1.94	1.96
E	1.96	1.97	1.98	2.00	1.95	1.94	1.97	1.98
F	1.96	1.99	1.99	1.99	1.96	1.97	1.98	1.97
G	1.98	1.95	**2.01**	2.00	1.97	1.96	1.99	**2.00**
H	1.95	1.98	1.96	1.98	1.95	1.96	1.99	**2.00**

Fig. 8. Fin total nuclear heating rate results for high flux position (5cm below core centerline) in four core loadings. Highest nuclear heating rates are shown in red and lowest in blue. All rates are a statistical combination of five random seed runs and are given in $W.g^{-1}$. 1σ uncertainties are 0.07 $W.g^{-1}$ for all fins.

	Reference Cell				Sample Cell			
Core	238	239	240	242	238	239	240	242
A	1.74	1.72	1.74	1.75	1.80	1.80	1.85	1.83
B	1.73	1.71	1.73	1.73	1.80	1.80	1.83	1.80
C	**1.70**	1.74	1.72	1.74	1.80	1.82	1.81	1.83
D	1.73	1.71	1.73	1.73	**1.76**	1.78	1.82	1.79
E	1.73	**1.70**	1.75	1.74	1.81	1.77	1.83	1.85
F	1.74	1.74	1.74	1.75	1.83	1.82	1.83	1.85
G	1.74	1.73	1.74	1.75	1.82	1.81	1.84	1.84
H	1.74	1.74	1.75	**1.76**	1.79	1.82	1.85	**1.87**

Fig. 9. Fin total nuclear heating rate results for low flux position (15cm below core centerline) in four core loadings. Highest nuclear heating rates are shown in red and lowest in blue. All rates are a statistical combination of five random seed runs and are given in $W.g^{-1}$. 1σ uncertainties are 0.07 $W.g^{-1}$ for all fins.

While the highest rates were observed in the tallies for the G and H fins in both cells in each position, the difference between the highest and lowest observed heating rate is within one standard deviation of the tally. Therefore, there is no statistically significant support for a spatial bias in the fins that might be observed over random variation. The same reasoning extends to the fins with the lowest observed heating rates, although the minimum values appeared across a larger set of fins B, C, D, and E.

V. Conclusions

The alignment of flux profiles and nuclear heating rate trends supports the early predictions of in-core response and affirms the reliability of the model results. The consistency within each problem run of nuclear heating rates, relative to the axial positioning also implies that the resulting nuclear heating rates are accurate inputs for the subsequent 3-D thermal calculations realized by AMU thanks to COMSOL Multiphysics software. It also suggests that with data measurements at a few points of interest, the shape of the resulting nuclear heating rates could be accurately estimated with interpolation. The magnitudes of the nuclear heating rates are all within the expected bounds of what has previously been measured and modelled for similar materials in similar irradiation conditions of MITR.

The lack of influence from core loading significantly simplifies the project analysis as it removes the necessity for re-performing calculations with the actual core loading at the time of irradiation or having to adjust the irradiation schedule or core plan to avoid unnecessary local effects. Likewise, the lack of evidence supporting a spatial bias in the fin orientation indicates that a rotation of the calorimeter during irradiation is not strictly necessary to obtain even heating and thermal transfer. These verifications increase confidence in the irradiation facility design and establishes a flexible envelope for obtaining different test measurements for calorimeter validation and verification.

Acknowledgment

The CALOR-I project leading to this publication has received funding from the Excellence Initiative of Aix-Marseille University - A*Midex, a French “Investissements d’Avenir programme”.

References

[1] A.Volte, M. Carette, A. Lyoussi, G. Kohse, J. Rebaud, V. Valero, C. Reynard-Carette, “Review of CALORRE Calorimeter Characterizations Under Laboratory and Irradiation Conditions”, IEEE Trans. Nucl. Sci., vol. 69, no. 4, pp. 840-848, April 2022, doi: 10.1109/TNS.2022.3150148

[2] MIT Nuclear Reactor Laboratory, “In-Core Experiments,” Facilities, https://nrl.mit.edu/facilities/in-core (accessed July, 2023).

[3] A. Volte, S. Hauptman, D. Carpenter, M. Carette, A. Lyoussi, G. Kohse, C. Reynard-Carette, “Characterization of a new reduced-height CALOREE differential calorimeter for CALOR-I Irradiation in MITR”, ANIMMA conference, Lucca, Italy, 2023.

[4] X-5 Monte Carlo Team, MCNP – A General Monte Carlo N-Particle Transport Code, Version 5, Volume II: User’s Guide. April 24, 2003.

[5] M.B. Chadwick, P. Obložinský, M. Herman, N.M. Greene, R.D. McKnight, D.L. Smith, P.G. Young, R.E. MacFarlane, G.M. Hale, S.C. Frankle, A.C. Kahler, T. Kawano, R.C. Little, D.G. Madland, P. Moller, R.D. Mosteller, P.R. Page, P. Talou, H. Trellue, M.C. White, W.B. Wilson, R. Arcilla, C.L. Dunford, S.F. Mughabghab, B. Pritychenko, D. Rochman, A.A. Sonzogni, C.R. Lubitz, T.H. Trumbull, J.P. Weinman, D.A. Brown, D.E. Cullen, D.P. Heinrichs, D.P. McNabb, H. Derrien, M.E. Dunn, N.M. Larson, L.C. Leal, A.D. Carlson, R.C. Block, J.B. Briggs, E.T. Cheng, H.C. Huria, M.L. Zerkle, K.S. Kozier, A. Courcelle, V. Pronyaev, S.C. van der Marck, "ENDF/B-VII.0: Next generation evaluated nuclear data library for nuclear science and technology", Nucl. Data Sheets 107(2006)2931.

[6] K. Sun, “Nuclear Heating Rate of Bounding Case FS-2 Design” Internal MIT Nuclear Reactor Laboratory Document. April 2014.